Supporting Information: Enrofloxacin Permeation Pathways across the Porin OmpC

Jigneshkumar Dahyabhai Prajapati,[†] Carlos José Fernández Solano,[†] Mathias Winterhalter,[‡] and Ulrich Kleinekathöfer[*,†]

[†]*Department of Physics and Earth Sciences, Jacobs University Bremen, 28759 Bremen, Germany*

[‡]*Department of Life Sciences and Chemistry, Jacobs University Bremen, 28759 Bremen, Germany*

E-mail: u.kleinekathoefer@jacobs-university.de

S1 Force field parameters for the enrofloxacin molecule

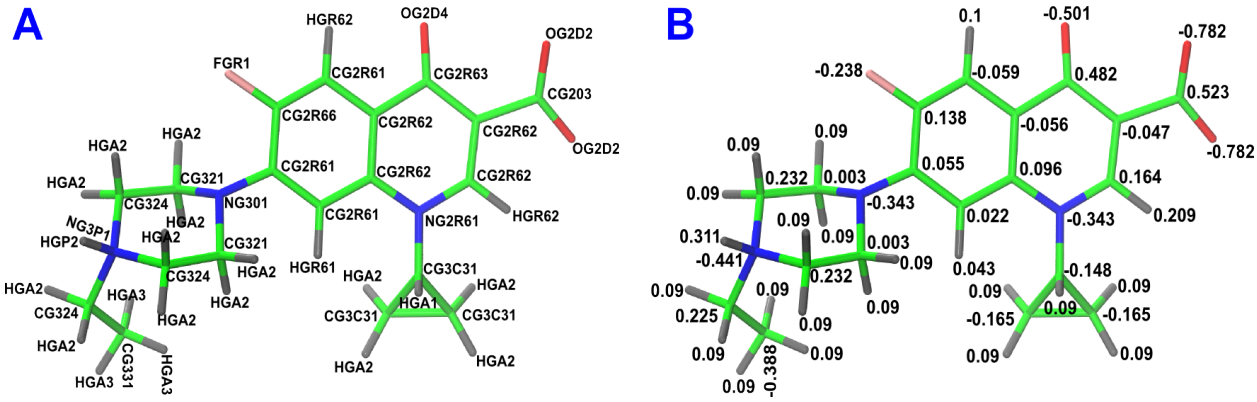

Figure S1: (A) Atom types and (B) optimized partial charges for the enrofloxacin molecule.

A similar strategy as for the ciprofloxacin molecule was used for optimizing the force field parameters for the enrofloxacin molecule. The initial force field parameters were obtained from the ParamChem webserver[1,2] based on the analogy with existing molecules in the CGenFF database.[3] An additional optimization was carried out using the VMD Force Field Toolkit (ffTK) plugin[4] for only those parameters for which a penalty score greater than 10 was assigned by the ParamChem webserver. The quantum calculations were performed using the Gaussian 9 package.[5] The optimized partial charges are listed in Table S1 and depicted in Fig. S1. Furthermore, the optimized bonded parameters are summarized in Table S2.

Table S1: Partial atomic charges for the enrofloxacin molecule. It should be noted that within the CHARMM parametrization procedure a charge of +0.09 is assigned to aliphatic hydrogen atoms by default.

Atom name	Atom type	CGenFF partial charge	Optimized partial charge
C1	CG2R61	-0.142	-0.059
C2	CG2R66	0.099	0.138
C3	CG2R61	0.493	0.055
C4	CG2R61	-0.116	0.022
H5	HGR62	0.266	0.100
F6	FGR1	-0.230	-0.238
H7	HGR61	0.169	0.043
C8	CG2R62	0.244	0.096
C9	CG2R62	-0.108	-0.056
C10	CG2R63	0.689	0.482
C11	CG2R62	-0.059	-0.047
C12	CG2R62	0.184	0.164
N13	NG2R61	-0.948	-0.343
O14	OG2D4	-0.477	-0.501
C15	CG2O3	0.650	0.523
H16	HGR62	0.111	0.209
C17	CG324	0.174	0.232
C18	CG321	-0.101	0.003
N19	NG301	-0.460	-0.343
C20	CG321	-0.101	0.003
C21	CG324	0.174	0.232
N22	NG3P1	-0.394	-0.441
H23	HGA2	0.090	0.090
H24	HGA2	0.090	0.090
H25	HGA2	0.090	0.090
H26	HGA2	0.090	0.090
H27	HGA2	0.090	0.090
H28	HGA2	0.090	0.090
H29	HGA2	0.090	0.090
H30	HGA2	0.090	0.090
C31	CG3C31	-0.093	-0.148
C32	CG3C31	-0.180	-0.165
C33	CG3C31	-0.180	-0.165
H34	HGA1	0.090	0.090
H35	HGA2	0.090	0.090
H36	HGA2	0.090	0.090
H37	HGA2	0.090	0.090
H38	HGA2	0.090	0.090
O39	OG2D2	-0.759	-0.782
O40	OG2D2	-0.759	-0.782
C41	CG324	0.180	0.225
C42	CG331	-0.269	-0.388
H43	HGA2	0.090	0.090
H44	HGA2	0.090	0.090
H45	HGA3	0.090	0.090
H46	HGA3	0.090	0.090
H47	HGA3	0.090	0.090
H48	HGP2	0.323	0.311

Table S2: Optimized bonded force field parameters for the enrofloxacin molecule.

Bond type	k_b [kcal/(mol Å^2)]	b_0 [Å]	
CG3C31-NG2R61	383.864	1.431	
Angle type	k_θ [kcal/(mol rad^2)]	θ_0 [°]	
CG2R62-CG2R63-CG2R62	208.080	117.771	
CG324-CG321-NG301	257.880	107.894	
CG3C31-CG3C31-NG2R61	71.402	118.791	
NG2R61-CG3C31-HGA1	48.710	117.934	
CG321-NG301-CG321	29.493	110.317	
Dihedral type	k_χ [kcal/mol]	n	δ [°]
CG2R66-CG2R61-NG301-CG321	1.369	2	180
CG2R66-CG2R61-NG301-CG321	0.593	4	0
CG324-CG321-NG301-CG2R61	1.673	1	180
CG324-CG321-NG301-CG2R61	0.150	2	0
CG324-CG321-NG301-CG2R61	2.057	3	0
NG301-CG321-CG324-NG3P1	0.415	3	0
CG321-CG324-NG3P1-CG324	0.375	3	0
CG331-CG324-NG3P1-CG324	2.912	1	0
CG331-CG324-NG3P1-CG324	0.080	3	0
NG2R61-CG3C31-CG3C31-CG3C31	1.897	3	180

S2 Definition of the CVs

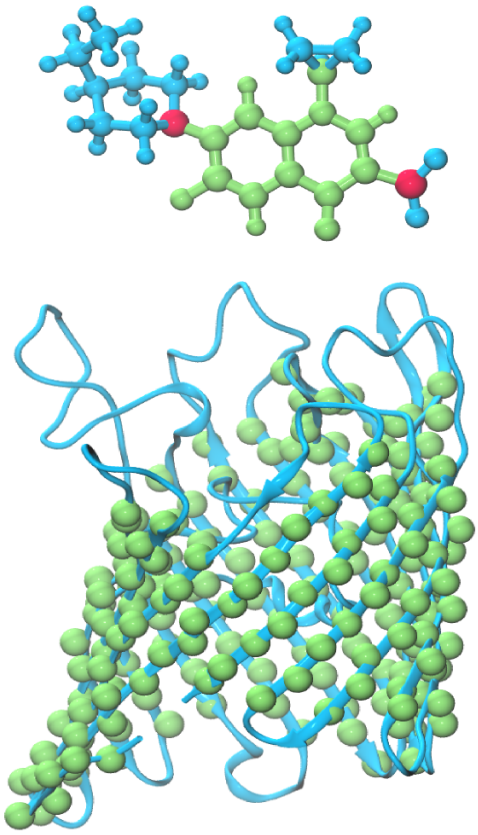

Figure S2: Description of the CVs z and z_{ij}. Concerning the CV z, the center of mass difference along the z-axis is calculated by choosing the C_α atoms from the OmpC monomer and the enrofloxacin atoms from the quinolone moiety (highlighted as green and read beads). The CV z_{ij} is defined as the z-component of an interatomic vector connecting two enrofloxacin selected atoms, shown as red beads. This CV indicates the rotation of the molecule and can easily be transformed into an angular variable.

S3 Multiple walker WTmetaD simulation

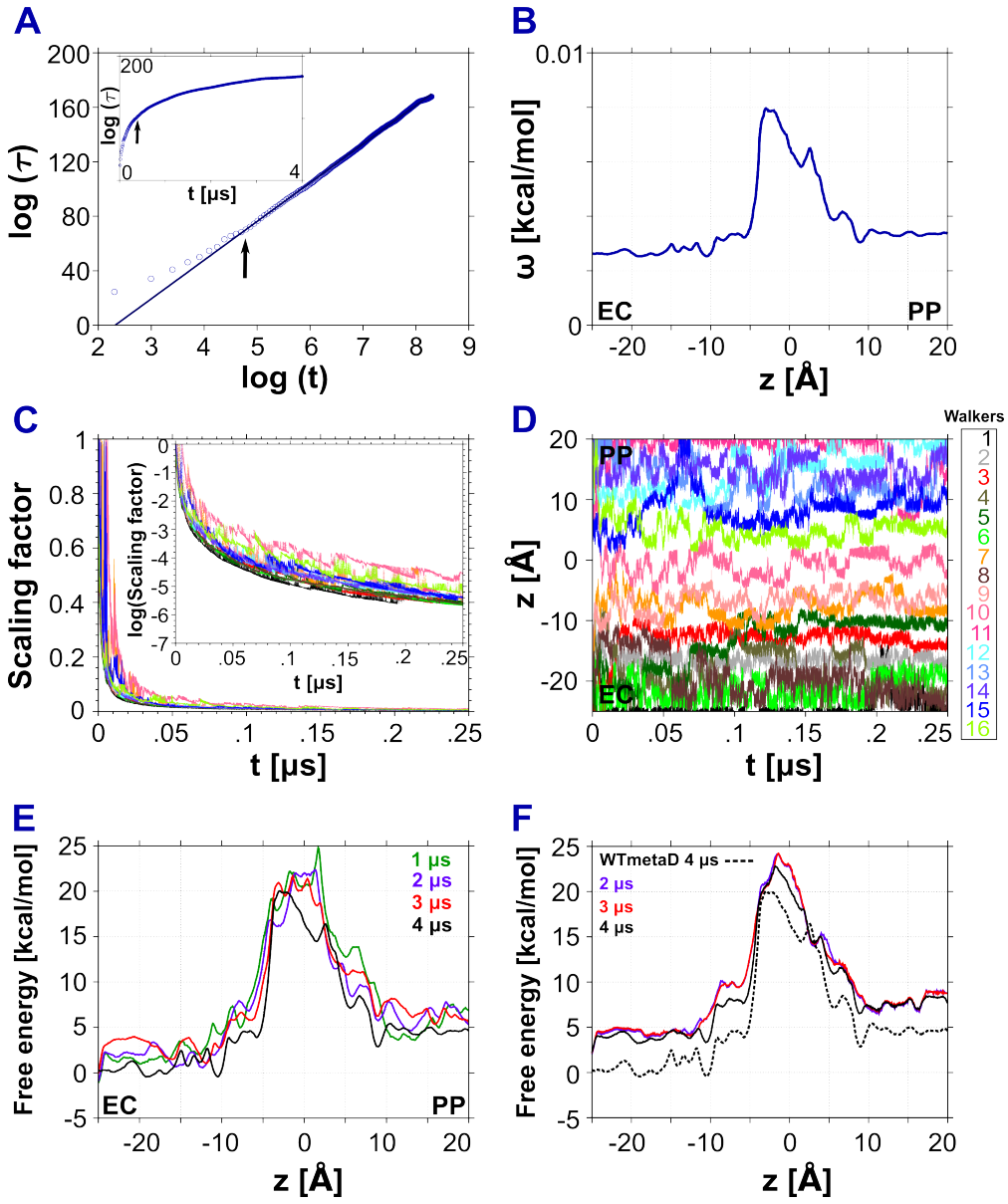

Figure S3: (A) Scaled time τ as a function the simulation time t on a log-log scale. The arrow indicates the time after which the asymptotic behavior $\log \tau \sim \gamma \log t$ is satisfied. The inset shows the same on a semi-logarithmic scale. (B) Scaled heights of the last deposited Gaussians in the CV space. (C) Scaling factor vs simulation time for each individual walker. The inset shows the same on a semi-logarithmic scale. (D) Time evolution of the CV z for each walker. (E) Time-independent FES estimates at several simulation times. (F) Reweighted FES estimates using the same CV z at several simulation times, as well as the time-independent FES estimates at 4 μs.

For the theoretical background on the convergence analysis, the interested reader is re-

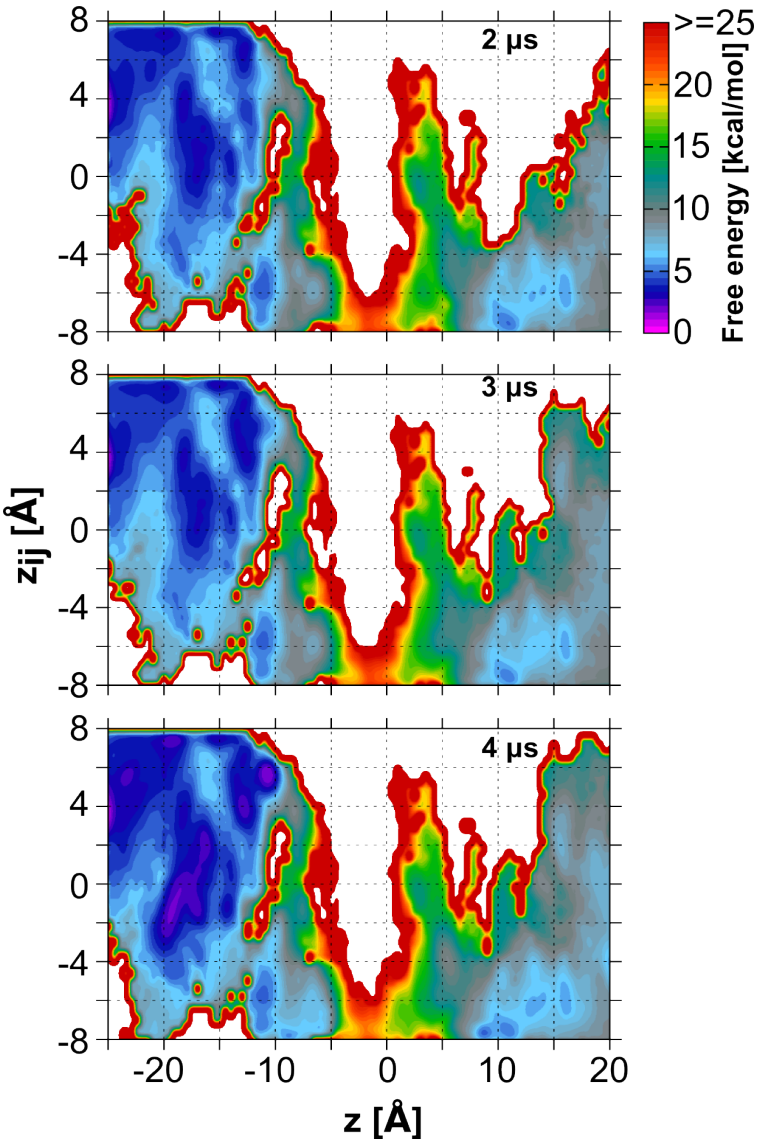

Figure S4: Reweighted FES estimate as a function of the CVs z and z_{ij} from the multiple walker WTmetaD simulation at different simulation times.

ferred to our previous study.[6] In Fig. S3A, the scaled time $\tau(t) = \int_0^t \exp\left(c(t')/k_B T\right) dt'$ is depicted as a function of the simulation time t on a log-log scale for the multiple walker WTmetaD simulation. Note that $c(t)$ is an estimator for the reversible work done by the bias, k_B denotes the Boltzmann constant and T the temperature. In the asymptotic limit $t \to \infty$, one obtains the relation[7] $\log \tau \sim \gamma \log t$, where $\gamma = (T + \Delta T)/T$ is the biasing factor and ΔT denotes the tuning temperature. Here, we focus on the $\log t$ range where $\log \tau$ exhibits a linear behavior. A Linear regression for this data range provides a slope

whose value is in excellent agreement with the biasing factor $\gamma = 30$, i.e., 28.5. This finding suggests that the quasistationary limit has been reached. Fig. S3B displays the scaled height $\omega_n = w \exp\left(-\frac{V_{n-1}(z_n)}{k_B \Delta T}\right)$ for the last deposited Gaussians in the CV space. To this end, we describe the CV space using a grid size of 0.1 Å. Note that w denotes the initial Gaussian height and $V_n(z)$ the bias potential evaluated at the z value for the nth iteration. As can be seen, the CV space is almost equally sampled and only small differences are observed in the constriction region, i.e., in $z \in [-5, 5]$ Å, where the main energy barriers are located (see below). This result means that the bias potential varies uniformly in the CV space and hence also supports the fact that the quasistationary limit has been reached. In Fig. S3C, we show the scaling factor $\exp\left(-\frac{V_{n-1}(z_n)}{k_B \Delta T}\right)$ applied for each walker in the CV space during the simulation. The scaling factor decays asymptotically and approaches zero without major oscillations, which means that the bias potential varies slowly after a transient period. Therefore, we can conclude that the quasistationary limit has been reached in the multiple walker WTmetaD simulation.

In Fig. S3D, the time evolution of the CV z for each walker is depicted for the multiple walker WTmetaD simulation. As can be observed, the entire CV space is explored and energy minima are visited many times. Thus, the simulation does not display any hysteresis since the bias potential grows evenly. A better sampling is accomplished outside the constriction whilst the main energy barriers are located in this region (see Figs. S3E and S3F). Moreover, Fig. S3E shows time-independent FES estimates at several simulation times for the multiple walker WTmetaD simulation. An acceptable convergence is achieved for most of the CV space. In Fig. S3F, we show the FES estimates extracted from the Tiwary-Parrinello reweighting procedure using the CV z at several simulation times for the multiple walker WTmetaD simulation, as well as the time-independent FES estimate at 4 μs. A remarkable agreement is achieved among the reweighted FESs at different simulation times. Based on the previous[6] and current study, we can claim that the reweighting procedure leads to better FES estimates than the time-independent FESs since the latter ones rely on a cancellation of

errors between two terms. To further substantiate this claim, it is worth mentioning that the reweighted FES as a function of the CVs z and z_{ij} from the multiple walker WTmetaD simulation shows very high convergence at different simulation times (see Fig. S4). In addition, a reasonable similarity is achieved between the reweighted and time-independent estimates, which is proposed as additional evidence for the convergence.[8] In summary, all these observations indicate a proper overall convergence of the free energy landscape obtained from the multiple walker WTmetaD simulation.

S4 Ciprofloxacin permeation across OmpC

The results in the Fig. S5 are extracted for our previous work.[6]

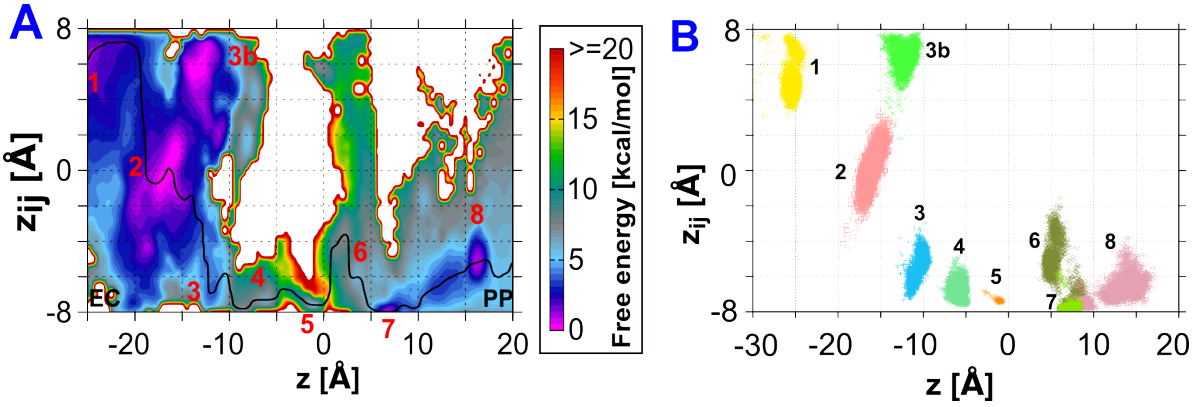

Figure S5: (A) Reweighted free energy landscapes as a function of the CVs z and z_{ij} from multiple walker WTmetaD simulation. The lowest-energy translocation pathway is depicted by a black line. (B) Distribution of the ciprofloxacin conformations in the CV space (z, z_{ij}) from unbiased MD simulations. Different colors have been used for the individual basins.

References

(1) Vanommeslaeghe, K.; MacKerell Jr, A. D. Automation of the CHARMM General Force Field (CGenFF) I: Bond Perception and Atom Typing. *J. Chem. Inf. Model.* **2012**, *52*, 3144–3154.

(2) Vanommeslaeghe, K.; Raman, E. P.; MacKerell Jr, A. D. Automation of the CHARMM General Force Field (CGenFF) II: Assignment of Bonded Parameters and Partial Atomic Charges. *J. Chem. Inf. Model.* **2012**, *52*, 3155–3168.

(3) Vanommeslaeghe, K.; Hatcher, E.; Acharya, C.; Kundu, S.; Zhong, S.; Shim, J.; Darian, E.; Guvench, O.; Lopes, P.; Vorobyov, I. et al. CHARMM General Force Field: A Force Field for Drug-like Molecules Compatible with the CHARMM All-atom Additive Biological Force Fields. *J. Comput. Chem.* **2010**, *31*, 671–690.

(4) Mayne, C. G.; Saam, J.; Schulten, K.; Tajkhorshid, E.; Gumbart, J. C. Rapid Parameterization of Small Molecules Using the Force Field Toolkit. *J. Comput. Chem.* **2013**, *34*, 2757–2770.

(5) Frisch, M. J.; Trucks, G. W.; Schlegel, H. B.; Scuseria, G. E.; Robb, M. A.; Cheeseman, J. R.; Scalmani, G.; Barone, V.; Mennucci, B.; Petersson, G. A. et al. Gaussian 09 Revision E.01. 2009; Gaussian Inc. Wallingford CT 2009.

(6) Prajapati, J. D.; Solano, C. J. F.; Winterhalter, M.; Kleinekathöfer, U. Characterization of Ciprofloxacin Permeation Pathways across the Porin OmpC Using Metadynamics and a String Method. *J. Chem. Theory Comput.* **2017**, *13*, 4553–4566.

(7) Tiwary, P.; Parrinello, M. A Time-independent Free Energy Estimator for Metadynamics. *J. Phys. Chem. B* **2014**, *119*, 736–742.

(8) Valsson, O.; Tiwary, P.; Parrinello, M. Enhancing Important Fluctuations: Rare Events

and Metadynamics from a Conceptual Viewpoint. *Annu. Rev. Phys. Chem.* **2016**, *67*, 159–184.